Article

Theoretical and Experimental Studies on the Mechanism of Norbornadiene Pauson#Khand Cycloadducts Photorearrangement. Is There a Pathway on the Excited Singlet Potential Energy Surface?

Santiago Olivella, Albert Sole#, Agusti# Lledo#, Yining Ji, Xavier Verdaguer, Rafael Suau, and Antoni Riera

J. Am. Chem. Soc., **2008**, 130 (50), 16898-16907 • DOI: 10.1021/ja802666v • Publication Date (Web): 18 November 2008

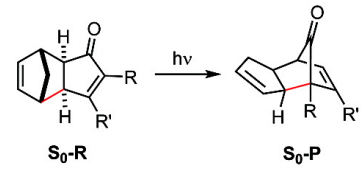

PHOTOCHEMICAL REARRANGEMENT

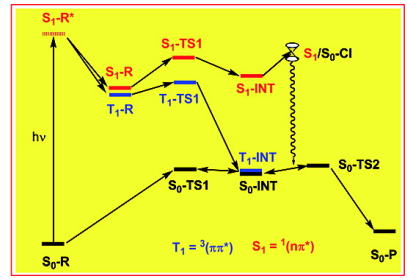

More About This Article

Additional resources and features associated with this article are available within the HTML version:

- Supporting Information
- Access to high resolution figures
- Links to articles and content related to this article
- Copyright permission to reproduce figures and/or text from this article

View the Full Text HTML

J|A|C|S
ARTICLES

Published on Web 11/18/2008

Theoretical and Experimental Studies on the Mechanism of Norbornadiene Pauson−Khand Cycloadducts Photorearrangement. Is There a Pathway on the Excited Singlet Potential Energy Surface?

Santiago Olivella,*,† Albert Solé,§ Agustí Lledó,‡ Yining Ji,‡ Xavier Verdaguer,‡ Rafael Suau,|| and Antoni Riera*,‡

Institut d'Investigacions Químiques i Ambientals de Barcelona, CSIC, Jordi Girona, 18-26, 08034-Barcelona, Catalonia, Spain, Departament de Química-Física i Institut de Química Teòrica i Computacional, Universitat de Barcelona, Martí i Franquès, 1−11, 08028-Barcelona, Catalonia, Spain, Departamento de Química Orgánica, Universidad de Málaga, 29071-Málaga, Spain, and Unitat de Recerca en Síntesi Asimètrica (URSA-PCB), Institute for Research in Biomedicine (IRB Barcelona) and Departament de Química Orgànica, Universitat de Barcelona, Parc Científic de Barcelona, Baldiri Reixac, 10, 08028-Barcelona, Catalonia, Spain

Received April 11, 2008; E-mail: sonqtc@cid.csic.es

Abstract: The intermolecular Pauson−Khand reaction (PKR), a carbonylative cycloaddition between an alkyne and an alkene, is a convenient method to prepare cyclopentenones. Using norbornadiene as alkene, a myriad of tricyclo[5.2.1.$0^{2,6}$]deca-4,8-dien-3-ones **1** can be easily prepared. The mechanism of the photochemical rearrangement of these adducts **1** into tricyclo[5.2.1.$0^{2,6}$]deca-3,8-dien-10-ones **2** has been studied. The ground state (S_0) and the three lowest excited states ($^3(\pi\pi^*)$, $^1(n\pi^*)$, and $^3(n\pi^*)$) potential energy surfaces (PESs) concerning the prototypical rearrangement of **1a** (the cycloadduct of the PK carbonylative cycloaddition of norbornadiene and ethyne) to **2a** have been thoroughly explored by means of CASSCF and CASPT2 calculations. From this study, two possible nonadiabatic pathways for the photochemical rearrangement arise: one starting on the $^3(\pi\pi^*)$ PES and the other on the $^1(n\pi^*)$ PES. Both involve initial C−C γ-bond cleavage of the enone, which leads to the formation of a bis-allyl or an allyl-butadienyloxyl diradical, respectively, that then decays to the S_0 PES through a $^3(\pi\pi^*)/S_0$ surface crossing or a $^1(n\pi^*)/S_0$ conical intersection, each one lying in the vicinity of the corresponding diradical minimum. Once on the S_0 PES, the ring-closure to **2a** occurs with virtually no energy barrier. The viability of both pathways was experimentally studied by means of triplet senzitization and quenching studies on the photorearrangement of the substituted Pauson−Khand cycloadduct **1b** (R = TMS, R′ = H) to **2b.** Using high concentrations of either piperylene as a triplet quencher, or benzophenone as a triplet sensitizer, the reaction rate significantly slowed down. A Stern−Volmer type plot of product **2b** concentration vs triplet quencher concentration showed an excellent linear correlation, thus indicating that only one excited state is involved in the photorearrangement. We conclude that, though there is a nonadiabatic pathway starting on the $^1(n\pi^*)$ PES, the reaction product is formed through the $^3(\pi\pi^*)$ state because the energy barrier involved in the initial C−C γ-bond cleavage of the enone is much lower in the $^3(\pi\pi^*)$ PES than in the $^1(n\pi^*)$ PES.

Introduction

The rich photochemistry of the enone functional group is still giving new useful and reliable reactions.[1−7] Besides the well-known [2 + 2] cycloaddition reaction, certainly the most applied photochemical reaction in organic synthesis,[2] and photochemical electron transfer reactions,[3] rearrangements are the most useful photochemical reactions.[4] Some of them involve the initial homolytic cleavage of sigma bonds, such as type B Zimmerman rearrangement[5] or the photochemical rearrangement of cyclopropene PK (Pauson−Khand) adducts into phenols that we described some years ago.[6] The Pauson−Khand reaction (PKR), a cobalt-catalyzed carbonylative [2 + 2 + 1] cycloaddition between an alkyne and an alkene (Scheme 1) is one of the best methods to prepare cyclopentenones.[7]

Scheme 1. The Intermolecular Pauson−Khand Reaction with Norbornadiene

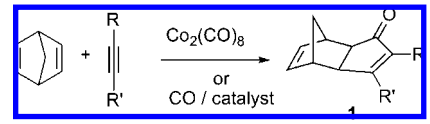

† CSIC.
§ Departament de Química-Física i Institut de Química Teòrica i Computacional, Universitat de Barcelona.
|| Universidad de Málaga.
‡ Unitat de Recerca en Síntesi Asimètrica (URSA-PCB), Institute for Research in Biomedicine (IRB Barcelona) and Departament de Química Orgànica, Universitat de Barcelona.

10.1021/ja802666v CCC: $40.75

Scheme 2. Photochemical Rearrangement of Norbornadiene PK Cycloadducts

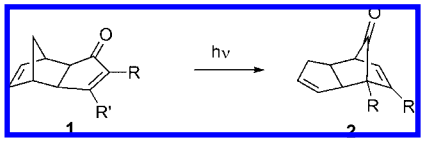

Although norbornadiene derivatives are the most useful intermolecular PK adducts,[8] their photochemistry has been studied only recently. We reported a new enone photoreaction by irradiation of cyclopentenones **1** at 350−360 nm which afforded the rearranged products **2** in good yields[9] (Scheme 2). The reaction is quite general for norbornadiene PK adducts since these compounds have the required exo stereochemistry necessary to prevent the known intramolecular [2 + 2] cycloaddition that takes place when the bicyclic enones have endo stereochemistry.[9,10]

A connectivity analysis revealed that a plausible mechanism for the transformation of a PK cycloadduct **1** into the rearranged product **2** would involve C−C γ-bond breaking of the enone to give a bis-allyl diradical intermediate **I**. The allylic nature of both fragments in the diradical intermediate **I** would facilitate the C4−C8 bond breaking (instead of C5−C6 bond cleavage) and would give enough stability to the intermediate to perform a conformational change via rotation about the linking C−C single bond. Thus, a new bond between the opposite sides of both allyl radicals should therefore be formed. The proposed reaction pathway is shown in Scheme 3.

Scheme 3. Proposed Reaction Pathway for the Photochemical Rearrangement

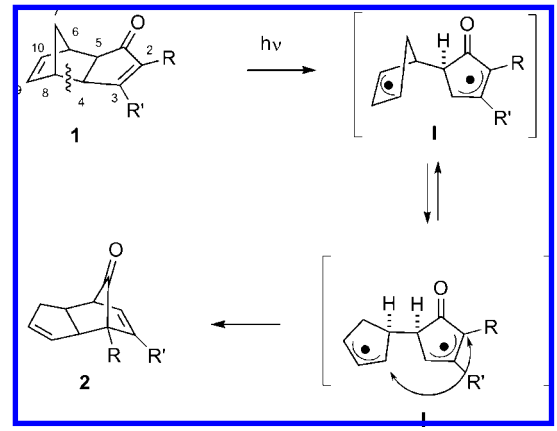

Assuming that this is the most likely reaction pathway, two important questions remain unanswered: What are the electronic states of the species involved in the reaction pathway? If the reaction occurs through an excited state, when does the radiationless decay to the singlet ground state occur? To answer these questions we undertook a detailed theoretical study of this reaction. We describe the results of this study in this paper.

Results and Discussion

Theoretical Calculations. Compound **1a** (R = R′ = H), the cycloadduct of the PK carbonylative cycloaddition of norbornadiene and ethyne, was taken as a model compound in our study since it is the simplest real compound that gives the reaction. To determine the electronic states involved in the photochemical rearrangement of **1a** to **2a**, we began with the computation of the equilibrium geometries of the ground-state singlet (S_0) and the three lowest excited electronic states ($^1(n\pi^*)$, $^3(n\pi^*)$, and $^3(\pi\pi^*)$) of both molecules.[11]

The geometries of other relevant stationary points (intermediates and transition states) on the S_0, $^1(n\pi^*)$, $^3(n\pi^*)$, and $^3(\pi\pi^*)$ potential energy surfaces (PESs) for the rearrangement of **1a** to **2a**, as well as the minimum energy point within the crossing seam of PES crossings, were also optimized. Selected geometrical parameters and the Cartesian coordinates of all structures reported in this article are available as Supporting Information (Figures S1−S8, Tables S1−S31). The nomenclature used for labeling the structures is composed of two parts. The first part of the label designates the electronic state and the second part indicates the nature of the structure, namely reactant (**R**), product (**P**), transition state (**TS**), intermediate (**INT**), conical intersection (**CI**), and surface crossing (**SC**). The transition structures are distinguished from each other by appending the numbers **1** and **2** as they are introduced.

Total electronic energies computed at the CASSCF and CASPT2 levels of theory, as well as the zero-point vibrational energies (ZPVEs), are collected in Table S32 (Supporting

(1) (a) Hoffmann, N. *Chem. Rev.* **2008**, *108*, 1052. (b) Griesbeck, A. G.; Mattay, J. *Mol. Supramol. Photochem.* **2005**, *12*, 1. (c) *CRC Handbook of Organic Photochemistry and Photobiology*, 2nd ed.; Horspool, W., Lenci, F., Eds.; CRC Press: Boca Raton, 2004.
(2) (a) Griesbeck, A. G.; Fiege, M. *Mol. Supramol. Photochem.* **2000**, *6*, 33. (b) Schuster, D. I.; Lem, G.; Kaprinidis, N. A. *Chem. Rev.* **1993**, *93*, 3. (c) Crimmins, M. T.; Reinhold, T. L. *Org. React.* **1993**, *44*, 297–588. (d) Crimmins, M. T. *Chem. Rev.* **1988**, *88*, 1453–1473.
(3) (a) Griesbeck, A. G.; Hoffmann, N.; Warzecha, K. *Acc. Chem. Res.* **2007**, *40*, 128. (b) Bertrand, S.; Hoffmann, N.; Pete, J. *Eur. J. Org. Chem.* **2000**, 2227. (c) Bertrand, S.; Hoffmann, N.; Humbel, S.; Pete, J. P. *J. Org. Chem.* **2000**, *65*, 8690. (d) Benko, Z.; Fraser-Reid, B.; Mariano, P. S.; Beckwith, A. L. J. *J. Org. Chem.* **1988**, *53*, 2066.
(4) (a) Horspool, W. M. *Photochemistry* **2007**, *36*, 23. (b) Margaretha, P. *CRC Handbook of Organic Photochemistry and Photobiology*, 2nd ed.; Horspool, W., Lenci, F., Eds.; CRC Press: Boca Raton, 2004; 76/1−76/12. (c) Winkler, J. D.; Lee, E. C. Y. *J. Am. Chem. Soc.* **2006**, *128*, 9040. (d) Zimmerman, H. E.; Nesterov, E. E. *J. Am. Chem. Soc.* **2003**, *125*, 5422. (e) Zimmerman, H. E.; Armesto, D. *Chem. Rev.* **1996**, *96*, 3065.
(5) (a) Zimmerman, H. E.; Sebek, P. *J. Am. Chem. Soc.* **1997**, *119*, 3677. (b) Zimmerman, H. E.; Epling, G. A. *J. Am. Chem. Soc.* **1972**, *94*, 3245. (c) Zimmerman, H. E.; Grunewald, J. O. *J. Am. Chem. Soc.* **1967**, *89*, 3354.
(6) (a) Gómez, I.; Olivella, S.; Reguero, M.; Riera, A.; Solé, A. *J. Am. Chem. Soc.* **2002**, *124*, 15375. (b) Marchueta, I.; Olivella, S.; Solà, L.; Moyano, A.; Pericàs, M. A.; Riera, A. *Org. Lett.* **2001**, *3*, 3197. The mechanism of this type of reaction has been the subject of some controversy. (c) Zimmerman, H. E.; Suryanarayan, V. *Eur. J. Org. Chem.* **2007**, 4091. (d) Gomez, I.; Reguero, M. *Mol. Phys.* **2006**, *104*, 889.
(7) Selected reviews:(a) Blanco-Urgoiti, J.; Anorbe, L.; Perez-Serrano, L.; Dominguez, G.; Perez-Castells, J. *Chem. Soc. Rev.* **2004**, *33*, 32. (b) Gibson, S. E.; Stevenazzi, A. *Angew. Chem., Int. Ed.* **2003**, *42*, 1800. (c) Brummond, K. M.; Kent, J. L. *Tetrahedron* **2000**, *56*, 3263. (d) Keun Chung, Y. *Coord. Chem. Rev.* **1999**, *188*, 297.
(8) (a) Bernardes, V.; Kann, N.; Riera, A.; Moyano, A.; Pericàs, M. A.; Greene, A. E. *J. Org. Chem.* **1995**, *60*, 6670. (b) Iqbal, M.; Evans, P.; Lledo, A.; Verdaguer, X.; Pericàs, M. A.; Riera, A.; Loeffler, C.; Sinha, A. K.; Mueller, M. J. *ChemBioChem* **2005**, *6*, 276. (c) Solà, J.; Revés, M.; Riera, A.; Verdaguer, X. *Angew. Chem., Int. Ed.* **2007**, *46*, 5020.
(9) Lledó, A.; Benet-Buchholz, J.; Solé, A.; Olivella, S.; Verdaguer, X.; Riera, A. *Angew. Chem., Int. Ed.* **2007**, *46*, 5943.
(10) (a) Suri, S. C.; Cabrera, A. C.; Wucherer, E. J.; Rodgers, S. L. *Synth. Commun.* **1997**, *27*, 841. (b) Zhu, J.; Klunder, A. J. H.; Zwanenburg, B. *Tetrahedron* **1995**, *51*, 5099.

(11) For the excited states, we follow the conventional notation of designating the lowest electronic excited states of conjugated α,β-unsaturated ketones in terms of orbital occupancy of the nonbonding lone pair orbital (n) of the oxygen atom and the highest occupied (π) and lowest unoccupied (π^*) orbitals of the ground-state π-system and the spin multiplicity (singlet or triplet).

Table 1. Vertical Excitation Energies (E_{vert}, kcal mol^{-1}) and Oscillator Strengths (f) Calculated with the 6-311G(d,p) Basis Set for the Lowest Excited States of **1a**[a]

	E_{vert}		
state	CASSCF(8,7)	CASPT2	f
$^1(n\pi^*)$	96.4	86.1	0.006
$^3(n\pi^*)$	91.4	80.2	
$^3(\pi\pi^*)$	93.6	90.9	

[a] Using the CASSCF(8,7)/6−311G(d,p) optimized geometry of the ground-state singlet.

Information). Vertical electronic excitation energies of the three lowest excited states of **1a**, calculated at both levels of theory, are given in Table 1. The CASSCF, CASPT2, and ZPVE-corrected CASPT2 relative energies of the equilibrium geometries, transition states, and intermediates located on the PES of each electronic state are summarized in Tables S34 and S35 (Supporting Information). The relative energies of the relevant conical intersection and surface crossing points between different PESs are given in Table S36 (Supporting Information).

Finally, the energy levels for all of the stationary points on the PES for each electronic state along an arbitrary reaction coordinate are schematically represented in Figure 1. The energy values were obtained from ZPVE-corrected CASPT2 energies relative to that of the ground state of **1a**.

A. Reactant and Product. At the CASSCF(8,7) level of theory the vertical electronic transition $S_0 \rightarrow {}^3(n\pi^*)$ is calculated to be the lowest vertical excitation energy of **1a** (Table 1). Interestingly, the calculated vertical excitation energy of the $^3(\pi\pi^*)$ state is only 2.2 kcal mol^{-1} higher than that of the $^3(n\pi^*)$ state. However, the CASPT2 calculations increase this energy difference to 10.7 kcal mol^{-1}. As regards the lowest singlet excited state of **1a**, namely the $^1(n\pi^*)$ state, it is remarkable that the vertical excitation energy of 86.1 kcal mol^{-1} calculated at the CASPT2 level of theory is in reasonable agreement with the low intensity absorption maximum at 341 nm (83.8 kcal mol^{-1}) observed in the UV spectrum of **1a**.[12] As expected for a symmetry forbidden $n \rightarrow \pi^*$ electronic transition, the value obtained for the corresponding oscillator strength is very small.

After the geometries are allowed to relax, the CASPT2 calculations (Table S34, Supporting Information) indicated that the $^3(n\pi^*)$ state still is the lowest energy excited state of **1a** but the $^3(\pi\pi^*)$ state lies only 1.2 kcal mol^{-1} above the energy of the $^3(n\pi^*)$ state. Inclusion of the ZPVE correction reduces this energy difference to 0.5 kcal mol^{-1}. In contrast, the $^3(\pi\pi^*)$ state was found to be the lowest energy excited state of **2a**, while the $^3(n\pi^*)$ state was predicted to be the second excited state. At the ZPVE-corrected CASPT2 level, the energy difference between these triplet states is 8.2 kcal mol^{-1}.

The C−O bond lengths calculated for the $^1(n\pi^*)$ and $^3(n\pi^*)$ states of **1a** (1.353 and 1.337 Å) and **2a** (1.350 and 1.334 Å) were found to be significantly longer than those calculated for the ground state of these species (1.200 and 1.188 Å). In contrast, the C−O bond lengths calculated for the $^3(\pi\pi^*)$ states (1.217 and 1.189 Å) are close to the values calculated for S_0. These results are ascribed to the fact that the $^1(n\pi^*)$ and $^3(n\pi^*)$ states arise from the S_0 state through excitation of one electron from the lone-pair n orbital of the oxygen atom to a π^* orbital which is C−O antibonding. Therefore, in the $^1(n\pi^*)$ and $^3(n\pi^*)$ states the C−O π bond is essentially broken. On the other hand, the $^3(\pi\pi^*)$ state arises from the S_0 state through a $\pi \rightarrow \pi^*$ excitation localized on a C=C fragment. This is reflected in the significantly long lengths calculated for the C2−C3 bond (1.512 Å) in **$^3(\pi\pi^*)$-R** and C8−C9 bond (1.493 Å) in **$^3(\pi\pi^*)$-P**, as compared to the lengths (1.341 and 1.336 Å) calculated for these bonds in **S_0-R** and **S_0-P**, respectively (see Figure 1 for atom numbering). Furthermore, the H−C2−C3−H dihedral angle in **$^3(\pi\pi^*)$-R** and the H−C8−C9−H dihedral angle in **$^3(\pi\pi^*)$-P** were found to be 58.4 and 114.7°, respectively, whereas in **S_0-R** and **S_0-P** these dihedrals angles were predicted to be ca. 0°.

The geometry of **S_0-P** compares well with that determined from the single crystal X-ray structure of **2b** (R = $(CH_3)_3Si$; R′ = H). Thus, the values of the most relevant bond lengths of **S_0-P** (C−O = 1.188 Å, C3−C4 = 1.345 Å, and C8−C9 = 1.336 Å) agree reasonably well with those (C−O = 1.203 Å, C3−C4 = 1.339 Å, and C8−C9 = 1.329 Å) determined for **2b**.[9]

To elucidate the mechanism of the photophysical process leading to the formation of the triplet states $^3(\pi\pi^*)$ and $^3(n\pi^*)$ of **1a** by radiationless decay after the initial photoexcitation $S_0 \rightarrow {}^1(n\pi^*)$, we searched for possible surface crossings in the region of the reactant. A $^1(n\pi^*)/^3(\pi\pi^*)$ surface crossing, designated by **$^1(n\pi^*)/^3(\pi\pi^*)$-SC** (Figure S3, Supporting Information), was located in the vicinity of structure **$^1(n\pi^*)$-R**. As expected for a singlet−triplet surface crossing between states with different electronic configurations, the spin−orbit-coupling (SOC) constant calculated at **$^1(n\pi^*)/^3(\pi\pi^*)$-SC** (Table S36, Supporting Information) appeared to be large (67.06 cm^{-1}), suggesting that intersystem crossing (ISC) at this point can be quite efficient. In contrast, all attempts to locate a $^1(n\pi^*)/^3(n\pi^*)$ surface crossing in the reactant region were unsuccessful. However, a conical intersection between the $^3(\pi\pi^*)$ and $^3(n\pi^*)$ PESs, designated by **$^3(\pi\pi^*)/^3(n\pi^*)$-CI** (Figure S3, Supporting Information), was located in the vicinity of structure **$^3(n\pi^*)$-R**. Consequently, the $^3(n\pi^*)$ PES can be easily accessed in the reactant region via initial ISC from the $^1(n\pi^*)$ to the $^3(\pi\pi^*)$ state followed by radiationless decay to the $^3(n\pi^*)$ state via internal conversion.

B. The Singlet Ground-State Potential Energy Surface. The thermal rearrangement of **1a** to **2a** on the S_0 PES is predicted to occur via a stepwise mechanism where the C4−C8 bond in

(12) At the CASPT2 level of theory the vertical excitation energy of the $^1(\pi\pi^*)$ state was calculated to be 149.5 kcal/mol (see Table S32, Supporting Information). Therefore, this excited singlet state was not further considered in this study.

(13) The common computational strategy to perform single-point CASPT2 calculations at CASSCF optimized geometries is only valid when the PESs described at both levels of theory behave more or less parallel with a constant relative influence of dynamic electron correlation. Therefore, the geometry optimization of these stationary points should be performed at the CASPT2 level of theory. Unfortunately, this type of calculation is still not practical for systems as large as $C_{10}H_{10}O$. To clarify this issue, the stationary points on the singlet ground-state PES were optimized by means of density functional theory calculations by using the spin-unrestricted version of the B3LYP functional[14] with the 6−311G(d,p) basis set. Nowadays it is generally accepted that the B3LYP functional accounts for most of the dynamic electron correlation energy, and therefore one would expect a reasonable description of the PES region where the bond breaking/making processes take place. The results of the B3LYP calculations (Table S33, Supporting Information) confirmed the stepwise mechanism found at the CASSCF level of theory for the thermal rearrangement of **S_0-R** to **S_0-P** on the ground-state PES. Furthermore, the geometries of the stationary points calculated with the B3LYP functional (Figure S5, Supporting Information) compare very well with the geometries of **S_0-TS1**, **S_0-INT**, and **S_0-TS2** optimized at CASSCF level of theory. More importantly, the bis-allyl diradical intermediate was calculated to lie 0.9 and 3.2 kcal mol^{-1} *below* the energies of the transition states found for the C4−C8 bond breaking and C2−C10 bond forming, respectively. Therefore, the B3LYP calculations predict the bis-allyl diradical to be a shallow minimum on the singlet ground-state PES.

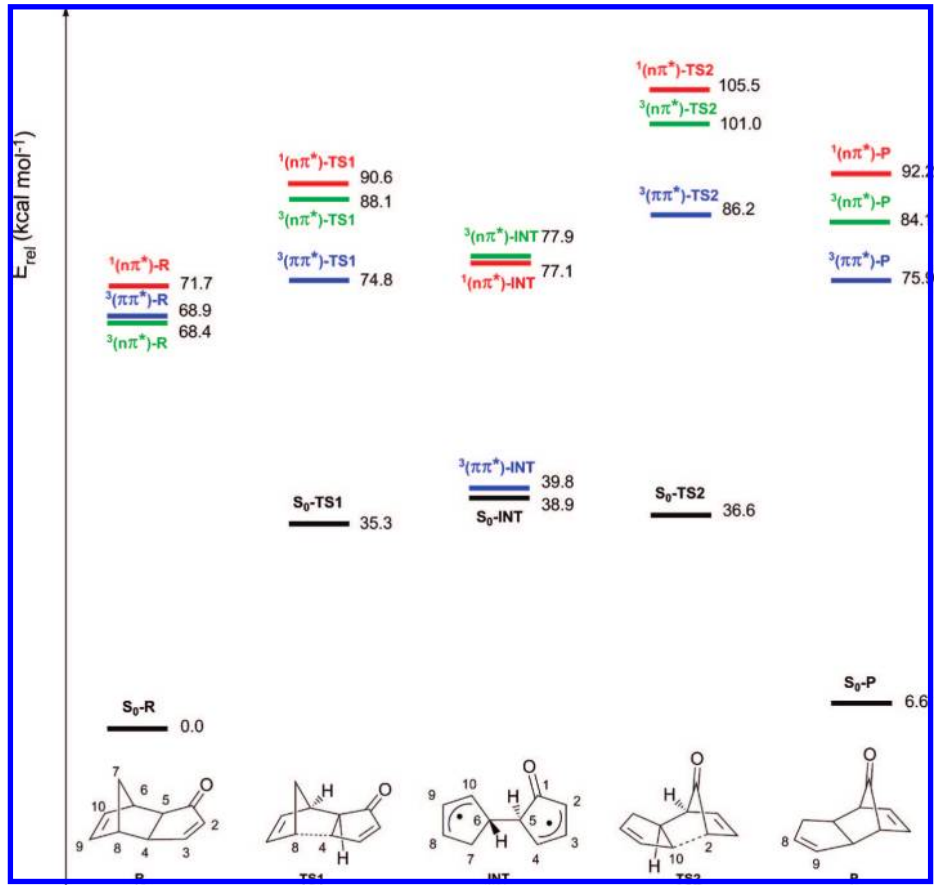

Figure 1. Energy levels of the stationary points on the PESs of the ground state (S_0) and the three lowest excited electronic states ($^1(n\pi^*)$, $^3(n\pi^*)$, and $^3(\pi\pi^*)$) associated with the adiabatic rearrangement of **1a** to **2a**. Relative energy values obtained from the ZPVE-corrected CASPT2/6−311G(d,p) total energies.

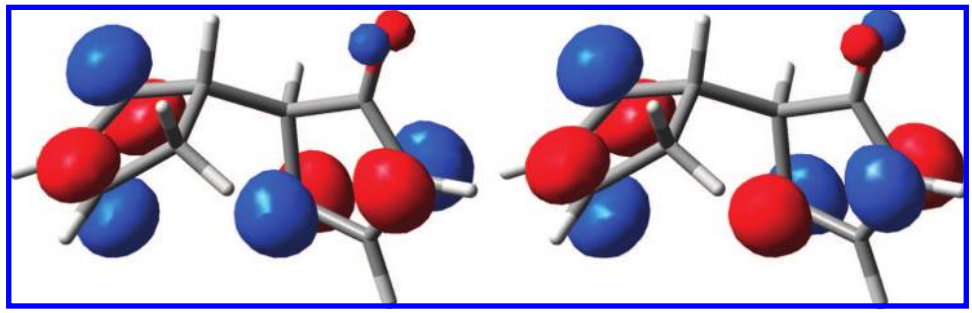

Figure 2. Representations of the natural orbitals having electron occupancies of 1.100 (left) and 0.903 (right) in the **S_0-INT** diradical intermediate.

S_0-R is cleaved first through a transition structure (**S_0-TS1**) leading to the formation of an intermediate (**S_0-INT**) (Figure 1). Subsequently, **S_0-INT** undergoes a rotation about the C6−C5 bond followed by the formation of the C2−C10 bond through a second transition state (**S_0-TS2**) yielding the product **S_0-P**. An inspection of the CASSCF natural orbitals calculated for **S_0-INT** revealed the presence of two orbitals with electron occupancies of 1.100 and 0.903. Basically, these singly occupied orbitals are the positive and negative combinations of two π-type orbitals: one of which is localized on the atoms C2 and C4, and the other on the atoms C8 and C10 (Figure 2). Therefore, the intermediate **S_0-INT** is a bis-allyl diradical with two unpaired electrons coupled to an overall open-shell singlet.

At the CASSCF level of theory, the C4−C8 bond cleavage in **S_0-R** via **S_0-TS1** leading to **S_0-INT** was predicted to be endoergic by 37.2 kcal mol^{-1} with an energy barrier of 39.4 kcal mol^{-1}, whereas the formation of the C2−C10 bond in **S_0-INT** through **S_0-TS2** to yield **S_0-P** was calculated to be exoergic by 30.7 kcal mol^{-1} and involved an energy barrier as low as 4.1 kcal mol^{-1} (Table S35, Supporting Information). However, at the CASPT2 level **S_0-INT** was calculated to lie 3.8 and 2.8 kcal mol^{-1} *above* the energies of **S_0-TS1** and **S_0-TS2**, respectively. This unexpected energy level ordering of **S_0-TS1**, **S_0-INT**, and **S_0-TS2** predicted by the CASPT2 calculations is most likely due to the sensitivity of the optimum geometries of these

(14) (a) Becke, A. D. *J. Chem. Phys.* **1993**, *98*, 5648. (b) Lee, C.; Yang, W.; Parr, R. G. *Phys. Rev. B* **1988**, *37*, 785. (c) Stevens, P. J.; Devlin, F. J.; Chablowski, C. F.; Frisch, M. J. *J. Phys. Chem.* **1994**, *98*, 11623.

(15) Compound **1b** (R = TMS, R′ = H) did not rearrange or decompose in *o*-dichlorobenzene at reflux (195 °C). When **1b** is heated in a solution of dioctyl ether at 250 °C, it slowly decomposes, but **2b** could not be detected in the reaction crude product.

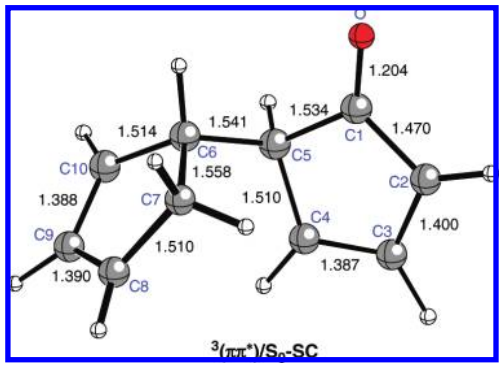

Figure 3. Selected bond lengths (Å) of the lowest-energy point on the surface crossing between the $^3(\pi\pi^*)$ and S_0 states optimized at the CASSCF/6−311G(d,p) level of theory.

stationary points to the inclusion of the dynamical valence-electron correlation.[13]

According to the ZPVE-corrected CASPT2 relative energies (Figure 1), the rearrangement of **S_0-R** to **S_0-P** is calculated to be endoergic by 6.6 kcal mol^{-1}, and the overall energy barrier is found to be at least as 36.6 kcal mol^{-1}. These results suggest that the thermal rearrangement of **1a** to **2a** could occur by heating at high temperature. However, from the experimental point of view, this approach was found to be not viable, mainly due to the volatility and low thermal stability of compound **2a**.[15]

C. The $^3(\pi\pi^*)$ Potential Energy Surface. The adiabatic rearrangement of **1a** to **2a** on the $^3(\pi\pi^*)$ PES also occurs stepwise via cleavage of the C4−C8 bond in **$^3(\pi\pi^*)$-R** through a transition structure (**$^3(\pi\pi^*)$-TS1**), leading to an intermediate (**$^3(\pi\pi^*)$-INT**), which may undergo ring closing through a second transition structure (**$^3(\pi\pi^*)$-TS2**) yielding **$^3(\pi\pi^*)$-P** (Figure 1). Interestingly, the geometry of the intermediate **$^3(\pi\pi^*)$-INT** was found to be nearly identical to that of the intermediate **S_0-INT**. Furthermore, an analysis of the CASSCF natural orbitals calculated for **$^3(\pi\pi^*)$-INT** indicated the presence of two orbitals, with electron occupancies of 1.003 and 1.000, which are virtually identical to the singly occupied natural orbitals of **S_0-INT** (Figure 2). Therefore, **$^3(\pi\pi^*)$-INT** is a bis-allyl diradical with the two unpaired electrons coupled to an overall triplet state, but these two electrons are far enough apart to be considered nearly uncoupled; hence, **S_0-INT** and **$^3(\pi\pi^*)$-INT** must be essentially degenerate. In fact, at the CASSCF level of theory, the energy difference between these structures was found to be only 0.1 kcal mol^{-1} and at the CASPT2 level the same energy difference rose to 1.0 kcal mol^{-1} (Table S35, Supporting Information).

According to Figure 1, the cleavage of the C4−C8 bond in **$^3(\pi\pi^*)$-R** via **$^3(\pi\pi^*)$-TS1** leading to **$^3(\pi\pi^*)$-INT** is calculated to be exoergic by 29.1 kcal mol^{-1} with an energy barrier of only 5.9 kcal mol^{-1}, whereas the formation of the C2−C10 bond in **$^3(\pi\pi^*)$-INT** through **$^3(\pi\pi^*)$-TS2** yielding **$^3(\pi\pi^*)$-P** is predicted to be endoergic by 36.1 kcal mol^{-1} and involves an energy barrier as high as 46.4 kcal mol^{-1}. This energy barrier appears to be too high to be in accordance with the experimental observation[9] that the photochemical rearrangement of **1a** to **2a** occurs easily at 15 °C and suggests that a surface hopping from the $^3(\pi\pi^*)$ to the S_0 PES via ISC may play a role. Accordingly, after C4−C8 bond cleavage in **$^3(\pi\pi^*)$-R** the molecule could undergo ISC to the S_0 PES, followed by ring-closure to **S_0-P**. In fact, a $^3(\pi\pi^*)/S_0$ surface crossing was located in the immediate vicinity of the diradical structure **$^3(\pi\pi^*)$-INT**. Figure 3 shows the geometry of lowest energy point on the seam of such surface crossing, designated by **$^3(\pi\pi^*)/S_0$-SC**. At the CASPT2 level, the energies of **$^3(\pi\pi^*)/S_0$-SC** and **$^3(\pi\pi^*)$-INT** were calculated to be essentially degenerate (Tables S35 and S36, Supporting Information). The SOC constant calculated at the **$^3(\pi\pi^*)/S_0$-SC** crossing point was predicted to be small (0.02), but the presence of the **$^3(\pi\pi^*)$-INT** minimum on the $^3(\pi\pi^*)$ PES means that ISC to S_o can indeed occur after many molecular vibrations.

A nonadiabatic reaction pathway, starting at the$^3(\pi\pi^*)$ PES, therefore, can be envisaged for the photorearrangement of **1a** to **2a**. The energy profiles of this pathway are depicted in Figure 4. It involves the initial population of **$^3(\pi\pi^*)$-R** via efficient ISC of the $^1(n\pi^*)$ to the $^3(\pi\pi^*)$ state through the **$^1(n\pi^*)/^3(\pi\pi^*)$-SC** surface crossing point (see Section A). Subsequently, **$^3(\pi\pi^*)$-R** undergoes cleavage of the C4−C8 bond via **$^3(\pi\pi^*)$-TS1** forming the triplet diradical **$^3(\pi\pi^*)$-INT**. At this point the molecule can then reach the **$^3(\pi\pi^*)/S_0$-SC** surface crossing point, where radiationless decay to the S_0 PES can occur through ISC. Once on the S_0 PES, the molecule can fall into the adjacent minimum **S_0-INT** and subsequently recouple the unpaired electrons on the C4 and C8 atoms to reform the reactant **S_0-R** with virtually no energy barrier. Alternatively the molecule can undergo a rotation about the C5−C6 bond and couple the unpaired electrons on the C2 and C10 atoms, with almost no barrier, to form the product **S_0-P**. This nonadiabatic reaction pathway is similar to that reported for the rearrangement of cyclopropene PK cycloadducts into phenols.[6]

D. The $^1(n\pi^*)$ and $^3(n\pi^*)$ Potential Energy Surfaces. The $^1(n\pi^*)$ and $^3(n\pi^*)$ PESs have comparable energies everywhere along the calculated reaction pathway for the rearrangement of **1a** to **2a**. On both PESs the adiabatic rearrangement is predicted to occur via a stepwise mechanism (Figure 1) where the C4−C8 bond is first cleaved through a transition structure (**$^1(n\pi^*)$-TS1** or **$^3(n\pi^*)$-TS1**) leading to the formation of an intermediate (**$^1(n\pi^*)$-INT** or **$^3(n\pi^*)$-INT**) which in turn undergoes ring-closure via a second transition state (**$^1(n\pi^*)$-TS2** or **$^3(n\pi^*)$-TS2**) to form the product (**$^1(n\pi^*)$-P** or **$^3(n\pi^*)$-P**).

As expected for two states with the same electronic configuration, the optimized geometries of the stationary points on the $^1(n\pi^*)$ and $^3(n\pi^*)$ PESs were found to be remarkably similar. This feature is especially true for the structures **$^1(n\pi^*)$-INT** and **$^3(n\pi^*)$-INT**, which have nearly identical geometry. Inspection of the CASSCF natural orbitals calculated for these structures revealed the presence of two orbitals with electron occupancies of 1.080 and 0.921 (**$^1(n\pi^*)$-INT**) and 1.001 and 0.999 (**$^3(n\pi^*)$-INT**). Basically, these singly occupied orbitals are a π-type orbital localized on the atoms C8 and C10 and an n-type orbital localized on the oxygen atom (Figure 5). Therefore, the intermediates **$^1(n\pi^*)$-INT** and **$^3(n\pi^*)$-INT** are allyl-butadienyloxyl diradical species in which there is almost no interaction between the unpaired electrons such that the singlet and triplet states differ only by the relative spins of these two electrons and must be nearly degenerate. In fact, at the CASSCF level of theory, the energy difference between **$^1(n\pi^*)$-INT** and **$^3(n\pi^*)$-INT** was calculated to be only 0.3 kcal mol^{-1}, and at the CASPT2 level, this energy difference rose to 0.8 kcal mol^{-1} (Table S35, Supporting Information). Consequently, **$^1(n\pi^*)$-INT** and **$^3(n\pi^*)$-INT** are the singlet and triplet states, respectively, of an allyl-butadienyloxyl diradical that lies some 38 kcal mol^{-1}

(16) A $^1(n\pi^*)/^3(n\pi^*)$ surface crossing, designated by **$^1(n\pi^*)/^3(n\pi^*)$-SC** (Figure S8, Supporting Information) was located in the vicinity of the diradical structures **$^1(n\pi^*)$-INT** and **$^3(n\pi^*)$-INT**. The SOC constant calculated at this crossing point appeared to be small (0.23 cm^{-1}).

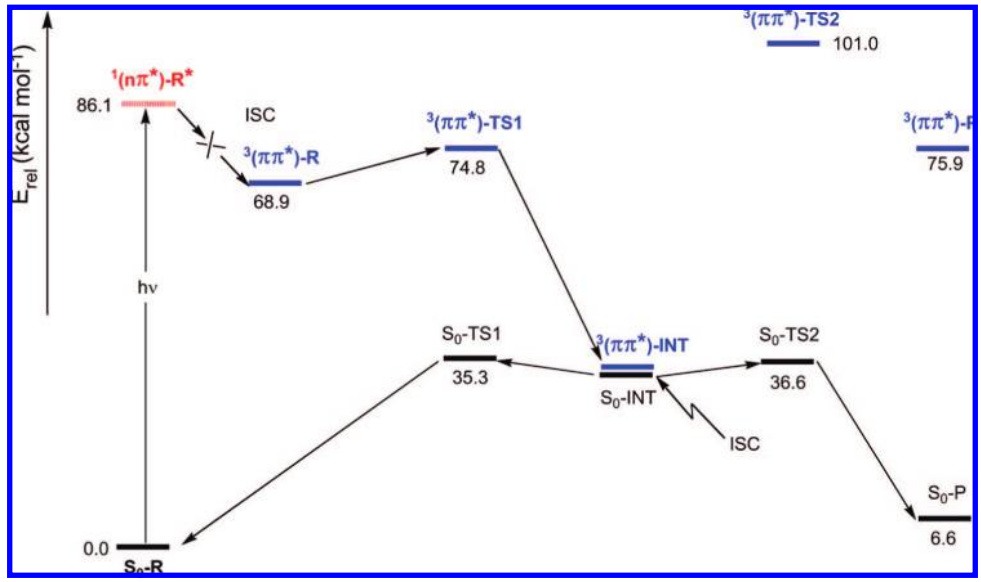

Figure 4. Energy profiles along an arbitrary reaction coordinate showing the pathway for rearrangement of **1a** into **2a** starting on the $^3(\pi\pi^*)$ PES. Relative energy values obtained from the ZPVE-corrected CASPT2/6−311G(d,p) total energies.

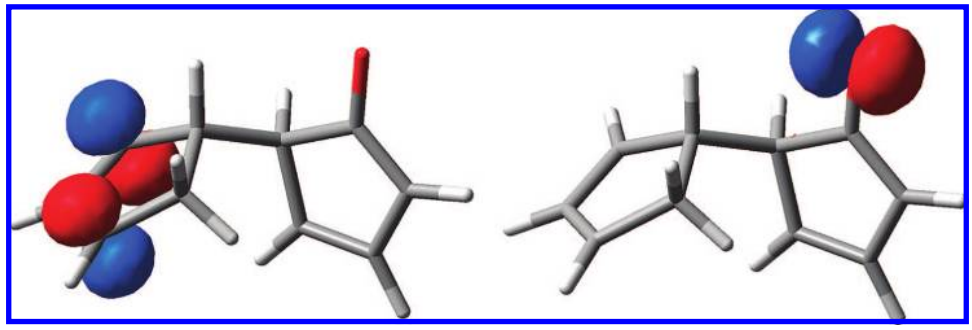

Figure 5. Representations of the natural orbitals having electron occupancies of 1.080 (left) and 0.921 (right) in the **$^1(n\pi^*)$-INT** diradical intermediate.

above the energy of the singlet and triplet structures (**S_0-INT** and **$^3(\pi\pi^*)$-INT**) of the bis-allyl diradical found on the S_0 and $^3(\pi\pi^*)$ PESs.[16]

As shown in Figure 1, the C4−C8 bond cleavage in either **$^1(n\pi^*)$-R** or **$^3(n\pi^*)$-R** through the transition structures **$^1(n\pi^*)$-TS1** or **$^3(n\pi^*)$-TS1** involves an energy barrier of 18.9 kcal mol^{-1} or 19.7 kcal mol^{-1}, respectively. Even in the unlikely case that **$^1(n\pi^*)$-R** and **$^3(n\pi^*)$-R** might contain an excess vibrational energy, these energy barriers seem too high to account for the experimental fact that the photochemical rearrangement of **1a** to **2a** occurs easily at 15 °C.[9] Furthermore, the subsequent ring-closure of either **$^1(n\pi^*)$-INT** to **$^1(n\pi^*)$-P** via **$^1(n\pi^*)$-TS2** or **$^3(n\pi^*)$-INT** to **$^3(n\pi^*)$-P** via **$^3(n\pi^*)$-TS2** involves an energy barrier of 28.4 or 23.1 kcal mol^{-1}, respectively (Figure 1), which is clearly too high as to be surmounted at 15 °C. Therefore, we investigated the possibility of surface hopping from the $^1(n\pi^*)$ to the S_0 PES. A $^1(n\pi^*)/S_0$ conical intersection was located in the region of **$^1(n\pi^*)$-INT**. Figure 6 shows the geometry of the lowest-energy point on such conical intersection, designated by **$^1(n\pi^*)/S_0$-CI**.[17]

Interestingly, the geometries of the cyclopentenyl moiety of **$^1(n\pi^*)/S_0$-CI** and **$^1(n\pi^*)$-INT** are virtually identical, while the geometries of the cyclopentadienyloxy moiety of these structures are significantly different. In particular, the C−O bond length in **$^1(n\pi^*)/S_0$-CI** (1.390 Å) is longer than in **$^1(n\pi^*)$-INT** (1.341 Å, Figure S7, Supporting Information). Thus, the passage from **$^1(n\pi^*)$-INT** to **$^1(n\pi^*)/S_0$-CI** occurs essentially via C−O stretching. This is illustrated in Figure 7, which is a schematic representation of the energy profiles of the S_0 and $^1(n\pi^*)$ states along the stretching of the C−O bond coordinate, based on the energies calculated at the CASSCF level. As a consequence of the double bond character of the carbonyl group at **S_0-INT** and the single bond nature of the C−O bond at **$^1(n\pi^*)$-INT**, the energy of S_0 rises more rapidly than that of $^1(n\pi^*)$ when the C−O distance increases. These energetic features are the main origin of the sloped conical intersection **$^1(n\pi^*)/S_0$-CI**.

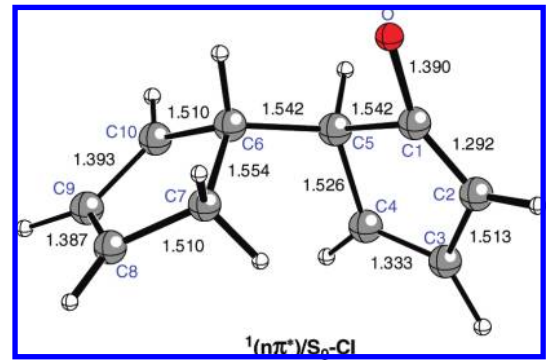

Figure 6. Selected bond lengths (Å) of the lowest-energy point on the conical intersection between the $^1(n\pi^*)$ and S_0 states optimized at the CASSCF/6−311G(d,p) level of theory.

From the reaction mechanism perspective, the most relevant energetic feature is that at the CASPT2 level of theory **$^1(n\pi^*)/$**

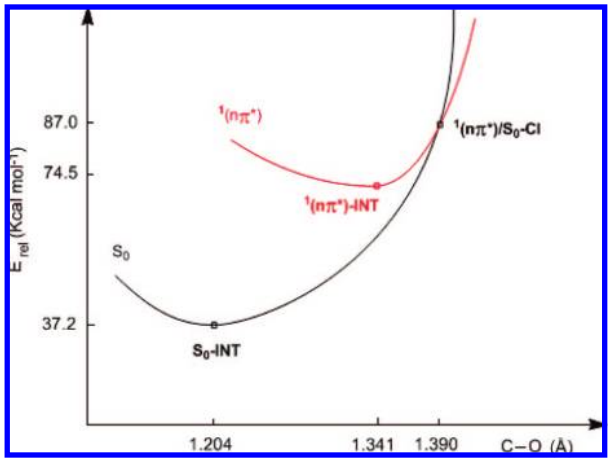

Figure 7. Schematic energy profiles of the S_0 and $^1(n\pi^*)$ states along the stretching C−O bond coordinate. Relative energy values obtained from the CASSCF/6−311G(d,p) total energies.

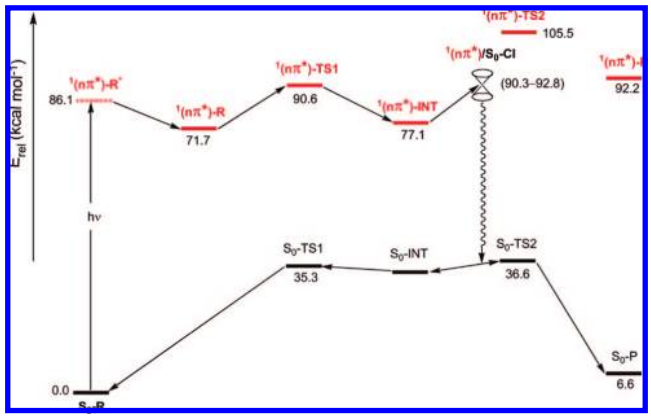

Figure 8. Energy profiles along an arbitrary reaction coordinate showing the pathway for rearrangement of **1a** into **2a** starting on the $^1(n\pi^*)$ PES. Relative energy values obtained from the ZPVE-corrected CASPT2/6−311G(d,p) total energies, except for **$^1(n\pi^*)$/S_0-CI** which were obtained from the CASPT2/6−311G(d,p) total energies.

S_0-CI was calculated to lie 16.7−18.9 kcal mol^{-1} below the energy of **$^1(n\pi^*)$-TS2**. Therefore, a nonadiabatic reaction pathway starting at the $^1(n\pi^*)$ PES can be proposed for the photorearrangement of **1a** to **2a**. The energy profiles corresponding to this pathway are depicted in Figure 8. It involves the initial electronic excitation from the ground-state equilibrium geometry **S_0-R** to an excited vibrational and rotational energy level of the $^1(n\pi^*)$ state, designated by **$^1(n\pi^*)$-R***, which according to the calculated vertical excitation energies (Table 1) lies no less than 86.1 kcal mol^{-1} above the energy of **S_0-R**. This vertical electronic excitation is followed by the cleavage of the C4−C8 bond through **$^1(n\pi^*)$-TS1** forming the singlet diradical **$^1(n\pi^*)$-INT**. At this point the carbonyl group can then undergo C−O stretch to reach the **$^1(n\pi^*)$/S_0-CI** conical intersection point, where fully efficient radiationless decay to the S_0 PES can occur via internal conversion. Once on the S_0 PES, the molecule can fall into the adjacent minimum **S_0-INT** and subsequently recouple the unpaired electrons on the C4 and C8 atoms to reform the reactant **S_0-R** with virtually no energy barrier. Alternatively the molecule can undergo a rotation about the C5−C6 bond and couple the unpaired electrons on the C2 and C10 atoms, with almost no barrier, to form the product **S_0-P**.

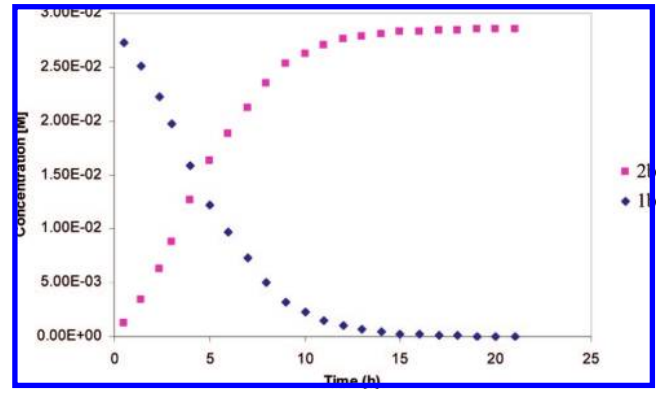

Figure 9. Reaction profiles of the photochemistry of **1b** in cyclohexane. Initial concentration of **1b**: 2.8 10^{-2} M. λ = 365 nm. Temperature: 15 °C.

Senzitization and Quenching Studies on the Mechanism of the Photorearrangement. According to the results of the theoretical calculations, after the initial vertical electronic transition $S_0 \rightarrow {}^1(n\pi^*)$ of the enone **1a**, two possible nonadiabatic pathways are envisaged for its photorearrangement to **2a**: one starting on the $^3(\pi\pi^*)$ PES and the other on the $^1(n\pi^*)$ PES. Both involve initial breaking of the C−C γ-bond of **1a** leading to the formation of a diradical intermediate (i.e., **$^3(\pi\pi^*)$-INT** or **$^1(n\pi^*)$-INT**, respectively) which decays to the S_0 PES through a $^3(\pi\pi^*)/S_0$ surface crossing or a $^1(n\pi^*)/S_0$ conical intersection, respectively. Once on the ground-state PES, the ring-closure to **2a** occurs with virtually no energy barrier in both pathways. Since the energy barrier involved in the breaking of the C−C γ-bond of **1a** is much lower in the $^3(\pi\pi^*)$ PES than in the $^1(n\pi^*)$ PES, it seems that the first mechanism should be the preferred one. Although well precedented, this mechanism might have as a possible drawback the low SOC constant calculated for the ISC to the singlet ground-state PES. On the other hand, though the formation of the diradical intermediate in the second mechanism involves surmounting a high energy barrier, the internal conversion of this diradical to the singlet ground-state PES through the $^1(n\pi^*)/S_0$ conical intersection might be easy. After a literature survey, we found a precedent of a related rearrangement for which a singlet excited-state pathway was also postulated.[18] In order to ascertain which of these two mechanisms is really working, we planned to perform the photorearrangement in the presence of a triplet sensitizer and a triplet quencher. The photochemical reactions were carried out on compound **1b** (R = TMS, R′ = H) because it is more accessible than **1a** and less volatile. The photochemical reactions were monitored by gas chromatography (GC). Figure 9 displays the plot of the concentration of both the reactant and product vs time for the transformation of **1b** into **2b**. As can be seen, in the initial parts of the reaction profiles the plots are straight lines, showing the expected asymptotic behavior after 7 h of reaction. The symmetry of both curves indicates a clean and complete transformation of the reactant into the product.

Once we had a good procedure for monitoring the reaction, we repeated it under the same conditions but with the addition

(17) A $^3(n\pi^*)/S_0$ surface crossing, designated by **$^3(n\pi^*)$/S_0-SC** (Figure S8, Supporting Information), was also located. The optimized geometries of **$^3(n\pi^*)$/S_0-SC** and **$^1(n\pi^*)$/S_0-CI** are nearly identical and the SOC constant calculated at the **$^3(n\pi^*)$/S_0-SC** crossing point appeared to be large (68.69 cm^{-1}).

(18) Ogino, T.; Wada, F.; Murayama, T.; Aoki, S.; Ohshima, K. *Tetrahedron Lett.* **1996**, *37*, 7065.

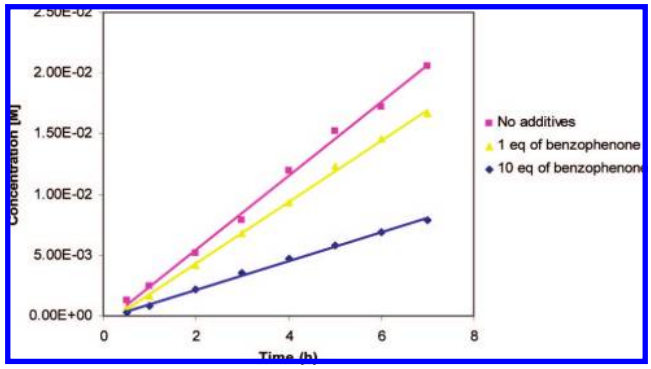

Figure 10. Reaction profiles of the photorearrangement of **1b** into **2b** with different concentrations of benzophenone as a triplet sensitizer. The plot shows molar concentration of product **2b** vs time. Initial concentration of **1b**: 2.8 10^{-2} M (cyclohexane). $\lambda = 365$ nm. Temperature: 15 °C.

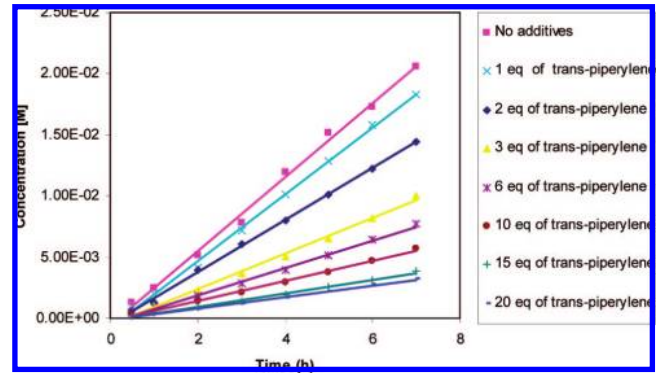

Figure 11. Reaction profiles of the photorearrangement of **1b** into **2b** with different concentrations of piperylene as a triplet quencher. The plot shows molar concentration of product **2b** vs time. Initial concentration of **1b**: 2.8 10^{-2} M (cyclohexane). $\lambda = 365$ nm. Temperature: 15 °C.

of 1 equiv of benzophenone as a triplet sensitizer. The plot of the product concentration vs time during the initial 7 h showed straight line ($R^2 = 0.9983$) for the photorearrangement, indicating a pseudo-zero-order reaction (Figure 10). As clearly seen in Figure 10, somewhat surprisingly, the reactions with 1 equiv of sensitizer and without it have very similar slopes, although reaction with benzophenone proceeded a little bit more slowly. To ensure that the triplet sensitizer was absorbing most of the light (>99%), we performed a reaction with 10 equiv of benzophenone. In this case, a significant reduction of reaction rate was observed (Figure 10), suggesting either the coexistence of singlet and triplet pathways or an inefficient energy transfer from triplet benzophenone to **1b.**

In order to ascertain if the mechanism through the excited singlet state was indeed contributing to the formation of **2b**, a further experiment was designed. The reaction was performed in the presence of 1 equiv of *trans*-1,3-pentadiene (*trans*-piperylene) as a triplet quencher.[18,19] In this case, when the additive acts as a quencher, it isomerizes to the photostationary mixture of cis/trans isomers. We were pleased to observe in the ^{1}H NMR spectrum of the crude reaction a substantial amount of cis isomer, clearly indicating that piperylene was acting as a quencher (Figure S9, Supporting Information). However, in the presence of 1 equiv of *trans*-piperylene, only a small decrease in the reaction rate was also observed (see Figure 11).

To find out whether we were using the right amount of quencher to completely inhibit the triplet pathway, we performed several photochemical reactions in the presence of increasing amounts of piperylene, and we monitored them by GC. As shown in Figure 11, the rates of the reaction slowed down as the concentration of the quencher increased.

It is generally assumed that if only one excited state is involved in a photochemical reaction, a Stern−Volmer plot of Φ^0/Φ (where Φ^0 is the quantum yield of the reaction and Φ is the quantum yield in the presence of quencher) vs the concentration of quencher shows a straight line.[20] Though we did not have quantum yield data, we used as a rough approximation the concentrations of the product **2b** after 4 h of reaction (results were coincident using any reaction time). Thus,

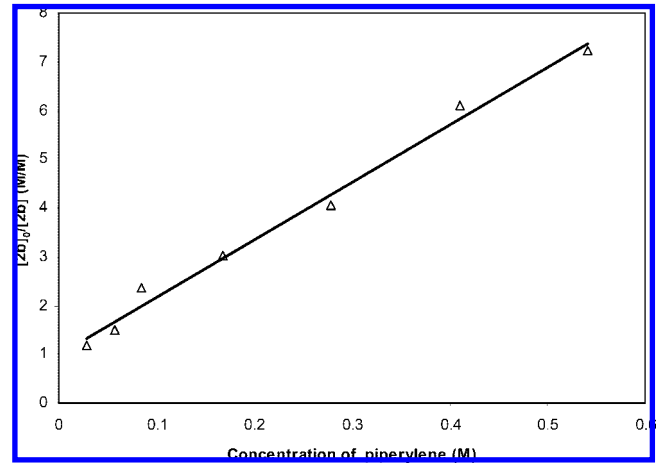

Figure 12. A Stern−Volmer type plot for the conversion of **1b** into **2b** after 4 h of reaction.

by plotting $[\mathbf{2b}]_0/[\mathbf{2b}]$ as a function of the concentration of quencher we obtained an excellent linear correlation ($R^2 = 0.9899$). This result clearly indicates that only the triplet excited state is involved in the photorearrangement of **1b** into **2b.** We conclude that, though there exists a nonadiabatic pathway starting on the $^1(n\pi^*)$ PES, most (if not all) of the reaction product is formed through the $^3(\pi\pi^*)$ state.

Summary and Conclusions

With the purpose of understanding the mechanism of the photorearrangement of norbornadiene Pauson−Khand cycloadducts, the singlet ground state (S_0) and the three lowest excited state ($^3(\pi\pi^*)$, $^1(n\pi^*)$, and $^3(n\pi^*)$) PESs concerning the prototype rearrangement of **1a** (R = H, R′ = H) to **2a** have been explored by means of CASSCF and CASPT2 calculations. There exists a stepwise adiabatic reaction pathway for the four PESs where the C−C γ-bond of **1a** is first broken, leading to an intermediate formed by two five-membered rings linked by a C−C single bond. Subsequently, a new C−C bond between the opposite sides of these rings is formed, yielding **2a** in the corresponding electronic state. The intermediate on both the S_0 and $^3(\pi\pi^*)$ PESs is a bis-allyl diradical, while on the $^1(n\pi^*)$ and $^3(n\pi^*)$ PESs is an allyl-butadienyloxyl diradical. The singlet state of the bis-allyl diradical is a shallow minimum on the S_0 PES lying about 40 kcal mol^{-1} above the energy of **1a**, suggesting that the thermal rearrangement of **1a** to **2a** should

(19) See, for instance: (a) Pelliccioli, A. P.; Klan, P.; Zabadal, M.; Wirz, J. *J. Am. Chem. Soc.* **2001**, *32*, 7931. (b) Smith, A. B., III; Wood, J. L.; Keenan, T. P.; Liverton, N.; Visnick, M. *J. Org. Chem.* **1994**, *22*, 6652. (c) Kimoto, K.; Tanabe, K.; Saito, S.; Umeda, Y.; Takimoto, Y. *Chem. Lett.* **1974**, *8*, 859.

(20) Turro, N. J. *Modern Molecular Photochemistry*; University Science Books: Sausalito, CA, 1991.

require heating at high temperature. Furthermore, the adiabatic reaction pathways on the $^3(\pi\pi^*)$, $^1(n\pi^*)$, and $^3(n\pi^*)$ PESs are not feasible at room temperature because the ring-closure of the diradical intermediates yielding **2a** involves an energy barrier ranging from 23.1 to 46.4 kcal mol^{-1}.

Two nonadiabatic pathways are found for the photochemical rearrangement: one starting on the $^3(\pi\pi^*)$ PES and the other on the $^1(n\pi^*)$ PES. Both involve initial formation of a diradical intermediate, which decays to the S_0 PES through a $^3(\pi\pi^*)/S_0$ surface crossing or a $^1(n\pi^*)/S_0$ conical intersection lying in the vicinity of the diradical minimum. Once on the S_0 PES, the ring-closure to **2a** occurs with virtually no energy barrier. These theoretical findings were experimentally investigated by means of triplet senzitization and quenching studies on the photorearrangement of the substituted Pauson−Khand cycloadduct **1b** (R = TMS, R′ = H) to **2b.** Using either high concentrations of benzopehnone as a triplet sensitizer or piperylene as a triplet quencher, the reaction rates significantly slowed down. However, a Stern−Volmer type plot using concentrations of the product performing the reaction with increasing amounts of pyperilene as triplet quencher, showed an excellent linear correlation. Our interpretation of these experiments is that the photorearrangement takes place through the $^3(\pi\pi^*)$ state because the energy barrier involved in the initial C−C γ-bond cleavage of the enone is much lower in the $^3(\pi\pi^*)$ PES than in the $^1(n\pi^*)$ PES.

Experimental Section

Details of the Computational Methods. The equilibrium geometries of the S_0, $^3(\pi\pi^*)$, $^1(n\pi^*)$, and $^3(n\pi^*)$ electronic states of **1a** and **2a** were optimized by carrying out multiconfigurational self-consistent field (MCSCF) calculations of the complete active space (CAS) SCF class[21] with the d,p-polarized triple split-valence 6−311G(d,p) basis set[22] using analytical gradient procedures.[23] The active space consisted of eight electrons and seven orbitals, which included the π and π^* orbitals of the two C═C fragments and the π, π^*, and n (the lone pair) orbitals of the C═O fragment. Distribution of the corresponding eight active electrons, namely, six π electrons and two n electrons, among these seven active orbitals leads to a CASSCF(8,7) wave function. The optimization of the geometries of the intermediates and transition states on the S_0, $^3(\pi\pi^*)$, $^1(n\pi^*)$, and $^3(n\pi^*)$ PESs for the rearrangement of **1a** to **2a** were also optimized at the CASSCF level of theory with the 6−311G(d,p) basis set. These optimizations required enhancing the CASSCF(8,7) by adding the pair of σ and σ^* orbitals of the C−C bond being broken at each reaction step, leading to a CASSCF (10,9) wave function. In order to obtain comparable energies, single point CASSCF(10,9) calculations were carried out for the S_0, $^3(\pi\pi^*)$, $^1(n\pi^*)$, and $^3(n\pi^*)$ states of **1a** and **2a** at their CASSCF(8,7) optimized geometries. All CASSCF calculations were performed state averaging over two states with equal weights except for the S_0 and $^3(\pi\pi^*)$ states, which were computed without state averaging.

All the stationary points were characterized by their harmonic vibrational frequencies as minima or saddle points. The harmonic vibrational frequencies were obtained by diagonalizing the mass-weighted Cartesian force constant matrix calculated numerically at the CASSCF level of theory with the 6−311G(d,p) basis set. The unscaled frequencies were used to compute the ZPVE corrections to the energies. Connections of the transition structures between designated minima were confirmed by intrinsic reaction coordinate (IRC) calculations[24] at the CASSCF/6−311G(d,p) level.

The investigation of a mechanism of a photochemical reaction involves, in addition to the study of ground- and excited-state reaction paths, a characterization of the regions where the PES crossings occur.[25] In these regions is where fast internal conversion or ISC are expected to take place. The minima on the crossing seam of singlet−singlet and triplet−triplet surface crossings (conical intersections)[25] and singlet−triplet surface crossings were optimized using the algorithm by Anglada and Bofill[26] within the formalism of the state-averaged MCSCF method at the CASSCF level of theory. A weighting of 50%/50% was assigned to the crossing states in the state-averaging procedure. In order to estimate the probability of ISC, the SOC constant between singlet and triplet states were calculated at the lowest-energy crossing points using a one-electron approximate spin−orbit Hamiltonian with the effective nuclear charges C: 3.6 and O: 5.6 optimized by Koseki et al.[27] For the SOC computations, state-averaged CASSCF orbitals were used.

To incorporate the effect of dynamical valence-electron correlation on the relative energy ordering of the excited states of **1a** and **2a**, as well as on the relative energy ordering of the stationary points and the lowest energy crossing points on the S_0, $^3(\pi\pi^*)$, $^1(n\pi^*)$, and $^3(n\pi^*)$ PESs, we performed second-order multiconfigurational perturbation theory calculations based on the CASSCF reference function (CASPT2).[28] CASPT2 single point energies were calculated at either CASSCF(8,7)/6−311G(d,p) (lower excited states of **1a** and **2a**) or CASSCF(10,9)/6−311G(d,p) (intermediates, transition states, and lowest-energy crossing points) optimized geometries using the 6−311G(d,p) basis set and all valence electrons were correlated. The best total energies correspond to the sum of the CASPT2/6−311G(d,p) energy and ZPVE correction.

The CASSCF geometry optimizations, vibrational frequencies, and IRC calculations were carried out with the GAUSSIAN 03 system of programs,[29] whereas the geometry optimization of the lowest energy crossing points of the conical intersections and singlet−triplet surface crossings, as well as the CASPT2 calculations, were performed with the MOLCAS 6.2 program package.[30]

Experimental Procedure. Photochemical reactions have been performed in a *Rayonet*-type apparatus equipped with 8 UV lamps (8W, 365 nm). A jacketed (water cooled, 15 °C) glass reactor fitted with two rubber septa and magnetic stirring was charged with **1b** (218 mg, 1 mmol) and benzophenone (184 mg, 1 mmol). Cyclohexane (35 mL, degassed bubbling nitrogen for 1 h) was added next. The flask was then flushed with nitrogen and irradiated at 365 nm while nitrogen was bubbled through the solution. The reaction was monitored by GC (HP-5, 30 m, gradient from 60 to 300 °C. t_R(**1b**) = 12.2 min, t_R(**2b**) = 11.8 min, t_R(benzophenone) = 13.3 min.). The same conditions were reproduced using 1, 2, 3, 6, 10, 15, and 20 equiv of *trans*-1,3-pentadiene (*trans*-piperylene) per mole of **1a**. In the case of the reaction with 1 equiv of *trans*-piperylene, the crude was analyzed by ^{1}H NMR ($CDCl_3$) after 24 h showing a 1:1.2 mixture of *cis/trans*-piperylene.

(21) For a review, see Roos, B. O. *Adv. Chem. Phys.* **1987**, *69*, 399.
(22) Krishnan, R.; Binkley, J. S.; Pople, J. A. *J. Chem. Phys.* **1980**, *72*, 650.
(23) (a) Schlegel, H. B. *J. Comput. Chem.* **1982**, *3*, 214. (b) Bofill, J. M. *J. Comput. Chem.* **1994**, *15*, 1.
(24) (a) Fukui, K. *Acc. Chem. Res.* **1981**, *14*, 363. (b) Ishida, K.; Morokuma, K.; Komornicki, A. *J. Chem. Phys.* **1977**, *66*, 2153. (c) Gonzalez, C.; Schlegel, H. B. *J. Chem. Phys.* **1989**, *90*, 2154. (d) Gonzalez, C.; Schlegel, H. B. *J. Phys. Chem.* **1990**, *94*, 5523.
(25) (a) Zimmerman, H. E. *J. Am. Chem. Soc.* **1966**, *88*, 1566. (b) Michl, J. *J. Mol. Photochem.* **1972**, 243. (c) Teller, E. *Isr. J. Chem.* **1969**, *7*, 227. (d) Bernardi, F.; Olivucci, M.; Robb, M. A. *Chem. Soc. Rev.* **1996**, *25*, 321.
(26) (a) Anglada, J. M.; Bofill, J. M. *J. Comput. Chem.* **1997**, *18*, 992. (b) De Vico, L.; Olivucci, M.; Lindth, R. *J. Chem. Theory Comput.* **2005**, *1*, 1029.
(27) Koseki, S.; Schmidt, M. W.; Gordon, M. S. *J. Phys. Chem.* **1992**, *96*, 10768.
(28) (a) Anderson, K.; Malmqvist, P.-A.; Roos, B. O.; Sadlej, A. J.; Wolinski, K. *J. Phys. Chem.* **1990**, *94*, 5483. (b) Anderson, K.; Malmqvist, P.-A.; Roos, B. O. *J. Chem. Phys.* **1992**, *96*, 1218.
(29) Frisch, M. J.; et al. Gaussian 03, revision C.01; Gaussian, Inc.: Wallingford, CT, 2004.

Acknowledgment. We thank the Spanish MEC (Grants CTQ2005-00623 and CTQ2005-07790) and the Catalonian AGAUR (Grant 2005SGR00111) for financial support. A.L. and Y.J. thank MEC for fellowships. The larger calculations described in this work were performed at the "Centre de Supercomputació de Catalunya" (CESCA). S.O. acknowledges gratefully the assistance of Drs. Isabel Gómez (Universitat Rovira i Virgili) and Lluis Blancafort (Universitat de Girona) with the use of GAUSSIAN 03 for CASSCF geometry optimizations of excited states. We thank two anonymous reviewers for helpful suggestions.

Supporting Information Available: Cartesian coordinates of all calculated structures, tables summarizing total and relative energies, and zero-point vibrational energies and ref 29 in full. This material is available free of charge via the Internet at http://pubs.acs.org.

JA802666V

(30) Karlström, G.; Lindh, R.; Malmqvist, P.-A.; Roos, B. O.; Ryde, U.; Veryazov, V.; Widmark, P.-O.; Cossi, M.; Schimmelpfennig, B.; Neogrády, P.; Seijo, L. *Comput. Mater. Sci.* **2003**, *28*, 222.